Journal of Sol-Gel Science and Technology
https://doi.org/10.1007/s10971-023-06127-5

INVITED PAPER: CHARACTERIZATION METHODS OF SOL-GEL AND HYBRID MATERIALS

Structural effects of TiO_2 nanoparticles in photocurable ladder-like polysilsesquioxane nanocomposites

Sandra Dirè[1] · Emanuela Callone[1] · Riccardo Ceccato[1] · Francesco Parrino[1] · Barbara Di Credico[2] · Silvia Mostoni[2] · Roberto Scotti[2] · Massimiliano D'Arienzo[2]

Received: 17 October 2022 / Accepted: 30 April 2023

Abstract

Ladder-like polysilsesquioxanes (LPSQs) are characterized by a double-stranded siloxane backbone, whose chemical and structural properties depend on both the synthesis parameters and the nature of the organic side-chains. In the case of ladder-like (methacryloxypropyl) polysilsesquioxanes (LPMASQ), polymer matrices can be produced by exploiting the presence of photocurable methacrylate groups. Consequently, they can be used to prepare functional nanocomposites (NCs), either by blending with organic polymers such as polybutadiene or exploiting the inorganic fillers' dispersion. Since the properties of LPMASQ-based NCs are strongly related to their structure, the structural changes of polymerized LPMASQ were investigated upon addition of low loadings of TiO_2 nanoparticles (up to 3 wt%) by solid state nuclear magnetic resonance and X-ray diffraction. The filler addition leads to the reduction of the polymerization capacity of the LPMASQ organic side-chains. Moreover, a different organization of ladder chains has been highlighted, ascribable to the increase in fully condensed linear ladder units at the expenses of folded chains and defective structures. The methodological approach here adopted can be extended to other composite systems and may help to describe the properties at the filler-matrix interface, offering valuable hints for a better design of these materials.

Graphical Abstract

The addition of TiO_2 to photocurable ladder-like poly(methacryloxypropyl silsesquioxanes) reduces the polymerization ability of the methacrylic groups, increases the amount of fully condensed linear ladders and affects the organization of the organic side-chains.

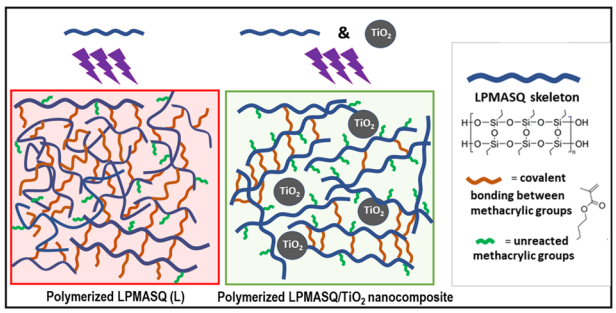

Supplementary information The online version contains supplementary material available at https://doi.org/10.1007/s10971-023-06127-5.

✉ Sandra Dirè
sandra.dire@unitn.it

✉ Emanuela Callone
emanuela.callone@unitn.it

[1] Department of Industrial Engineering and "Klaus Müller" Magnetic Resonance Lab., University of Trento, via Sommarive 9, 38123 Trento, Italy

[2] Department of Materials Science, INSTM, University of Milano-Bicocca, Via R. Cozzi 55, 20125 Milano, Italy

Published online: 22 May 2023

Keywords Ladder-like polysilsesquioxanes · Methacrylate groups · TiO_2 · NMR · XRD · Structural properties

Highlights

- LPMASQ/TiO_2 nanocomposites were produced by photopolymerization.
- According to ^{13}C NMR, LPMASQ polymerization decreases with increasing TiO_2 content, regardless of particles functionalization.
- ^{29}Si NMR shows that the percentage of fully condensed linear species increases with TiO_2 loading with respect to folded/defective chains.
- XRD evidences the effect of TiO_2 on the distribution of distances correlated to polymerized organic side chains.

1 Introduction

Polysilsesquioxanes (PSQs) are well-known silicon-based materials characterized by the repeating $[R\text{-}SiO_{1.5}]_n$ structural unit, where R could be either a polar or nonpolar, reactive or non-reactive organic functional group [1–5]. Moreover, they are characterized by a variety of structural patterns, which make PSQs a very versatile family of organic–inorganic hybrid materials [6–9]. Three main architectures are generally reported, i.e. random branched, polyhedral oligomeric silsesquioxanes (POSS), and ladder-like polysilsesquioxanes (LPSQs) [10]. A wide variety of POSS cages $(RSiO_{1.5})_n$, with n ranging from 6 to 18 have been synthesized, with various R groups [3, 11–13] and many of them are available for purchase nowadays.

LPSQs are characterized by an inorganic double-stranded backbone. They have rapidly become interesting competitors of POSS and linear polysiloxane, as blend components or fillers in nanocomposites (NCs), due to the tunable aspect ratio of the backbone and the various organic side-chains, which impart interesting physical properties [14], such as good thermal stability [15–17], chemical resistance to acids, excellent mechanical properties (e.g. high modulus, hardness) [14, 18, 19], and optical transparency [20]. Due to the large choice of R groups, LPSQs show high solubility in different solvents [21, 22], thus favouring their use in many applications. With the development of less time consuming synthesis methods that allow LPSQs production in good yield, they have been used in blends to increase thermal resistance and mechanical properties of organic polymers, such as polylactic acid [17, 23–25] or polyimide [26, 27], and to produce membranes for gas separation, hard coatings, self-healing and photosensitive materials, electrolytes in Li batteries and triboelectric generators [6, 15, 18, 20, 22, 28–30].

LPSQs can be synthesized by hydrolysis-condensation of organosilanes under acid or basic conditions, and their chemical-physical properties such as molecular weight, degree of structural order and crystallinity strongly depend on both synthesis conditions and nature of the organic group linked to silicon [10]. Phenyl-silsesquioxanes with different degrees of ordering were produced by varying time and temperature of aging, and using different templating agents, and their thermal stability was correlated with the amount of uncondensed silanols;[31] highly regular ladder polyphenylsilsesquioxanes with high molecular weight were prepared by Zhang et al. [32] using template alkoxysilane monomers in a three-step approach, concluded by an end-capping reaction.

Lee et al. proposed an easy synthetic method using K_2CO_3 as a mild base catalyst in water/THF mixture to obtain at room temperature either Phenyl-POSS or ladder-like polyphenylsilsesquioxane depending on the initial concentrations of phenyltrimethoxysilane [33–35]. Different photo-curable ladder polysilsesquioxanes were obtained [34] varying the ratio of rigid and flexible organic side-groups, namely phenyl and propylmethacrylate groups, obtaining structures with variable molecular weight. Later, the same approach was applied to the synthesis of ladder-like poly(methacryloxypropyl)silsesquioxane (LPMASQ) by hydrolysis-condensation of 3-methacryloxypropyl trimethoxysilane (MPTMS) [7, 36], leading to amorphous fully-condensed, medium-degree order ladder structures with MW ~ 28000 Da.

We have previously reported on the use of LPMASQ as active molecular fillers in the preparation of polybutadiene-based NCs for improving polybutadiene (PB) thermal and mechanical behaviour [37]. LPMASQ was prepared by reacting MPTMS under basic conditions in a one-pot procedure following the approach of Lee et al. [36] and its structural properties were confirmed by infrared and nuclear magnetic resonance spectroscopies. Nanocomposites were prepared by solvent-casting and photo-induced polymerization and we analysed in detail the structural organization of ladders in the elastomeric matrix. Increasing the amount of filler in the PB matrix, polymerization of methacrylate groups leads to gradual assembly of LPMASQ units and produced peculiar dielectric properties along with enhanced thermal and mechanical stability of the final nanocomposites [37].

Exploiting the dispersibility of oxide nanoparticles (NPs) in LPMASQ, it is possible to add new features or further vary the physical properties of the NCs. This approach was recently

exploited by our group to modify the surface wettability of PB/LPMASQ NCs obtained by photopolymerization [38] through the addition of MPTMS-functionalized silica nanoparticles. A similar approach was used to produce PB/LPMASQ NCs with active-passive O_2-scavenging ability by adding bare and MPTMS-modified TiO_2 nanoparticles [39]. Nanocomposites produced with modified TiO_2 showed an oxygen uptake rate much higher than that obtained with bare TiO_2. This result was discussed based on different mechanistic aspects, namely the production of singlet oxygen favoured by energy transfer mechanisms on the surface of functionalized titania.

In such studies, while a clear assessment of the effective role of LPMASQ for the achievement of peculiar functional properties was provided, the structural modifications of these units as a consequence of the interactions with filler particles was not investigated in detail. As concerns the use of titania NPs, besides imparting peculiar features to the composites, they may in principle influence the LPMASQ photocuring reaction, as recently pointed out for other acrylic and methacrylic systems, [40 and reference therein] where their capability to act as photoinitiators, generating reactive radicals under photoexcitation, has been exploited to produce self-curing composites. However, the possible structural changes derived from photopolymerization of LPMASQ UV-curable ladder-like units in the presence of TiO_2 have not been explored so far in the literature.

In this scenario, the present work aims at unveiling the structural effects imparted by titania addition to LPMASQ in NCs obtained by photopolymerization. In detail, LPMASQ and commercial TiO_2 NPs, either naked or surface-functionalized with MPTMS were employed as a suitable matrix and filler, respectively, for producing a NC by a simple and rapid solvent-casting technique followed by UV curing. A comprehensive structural investigation of the TiO_2 modified LPMASQ composites was performed by X-Ray Diffraction (XRD), attenuated total reflectance Fourier transform infrared (ATR-FTIR) spectroscopy and solid state nuclear magnetic resonance (NMR) spectroscopy, focusing on the effects of filler incorporation on the molecular organization. The results, besides evidencing a hindering effect of TiO_2 NPs on the curing efficacy, indicate a remarkable impact of the NPs on the structural features of both ladder backbones and organic side chains, shedding light on the properties at the hybrid interface and providing suitable information to better design these composite materials.

2 Experimental

2.1 Materials

3-Methacryloxypropyltrimethoxysilane (MPTMS, 98%) was supplied from ABCR GmbH (Germany). Benzophenone (≥99.0%), potassium carbonate (K_2CO_3, ≥99.0%), anhydrous toluene (99.8%), tetrahydrofuran (THF, 99.9%) and ethanol (96%) were purchased from Sigma–Aldrich. Irgacure 184 was supplied by Ciba. Titania NPs (Evonik Aeroxide P25, average particle size 30–50 nm, $SSA_{BET} = 54.7\ m^2g^{-1}$) were obtained from Evonik. All reagents were used without further purification.

2.2 Synthesis procedures

The preparation of LPMASQ (Scheme 1a) was carried out according to our previous reports [37–39] by MPTMS hydrolysis-condensation in the presence of K_2CO_3 catalyst in H_2O/THF mixture, adapting the procedure of Lee et al. [36]. In detail, MPTMS (0.08 mol) was added dropwise under nitrogen flow and vigorous stirring to a solution prepared by dissolving K_2CO_3 (0.04 g) in deionized H_2O (4.8 ml) and THF (9 ml). The clear solution was stirred at RT for 240 h in the dark, and after solvent evaporation under reduced pressure at 30 °C yielded a transparent and jelly-like product. ^{1}H, ^{13}C and ^{29}Si NMR (Online Resource Fig. S1 and experimental conditions), ATR-FTIR (Fig. S2) and thermogravimetric (TG) analyses (Fig. S3) were recorded to confirm the ladder-type structure of LPMASQ, in agreement with previous reports [36–38].

TiO_2 functionalization was performed as schematized in Fig. S4, using the procedure reported in [39]. MPTMS (0.063 mol) was slowly added under vigorous stirring to the dispersion of 0.006 mol of TiO_2 in 50 ml of toluene. The dispersion was refluxed (120 °C) for 16 h in the dark. Functionalized titania NPs (fTiO2) were recovered by centrifugation at 5000 revolutions per minute (rpm) for 10 min, washed three times with ethanol, and dried overnight at 80 °C. The particles functionalization was evaluated by FTIR spectroscopy (Fig. S5) and the amount of grafted molecules was calculated by TG analysis [39].

The synthesis of LPMASQ/titania NCs was performed according to [39] using a solvent casting technique followed by UV-induced photo-crosslinking (Scheme 1b). Briefly, LPMASQ (1 g) was dissolved in toluene (3 mL) at RT and various amounts of both TiO_2 and fTiO2 NPs were added to the solution to finally obtain NCs with 0, 1, 2, or 3 wt% NPs loadings. To improve the curing efficiency, both Irgacure 184 (1 wt%) and benzophenone (1 wt%) were used as photoinitiators [41]. After stirring under nitrogen in the dark for 16 h, the mixtures were cast in Teflon molds (internal diameter 4 cm) and heated at 70 °C for 1 h. The samples were photopolymerized under N_2 flow for 50 min by using a mercury vapor lamp (OSRAM, HBO 50 W/AC 39 V, lamp-sample distance 12 cm). The produced samples were stored in the dark under N_2 atmosphere. NCs are respectively labeled L_xTiO2 and

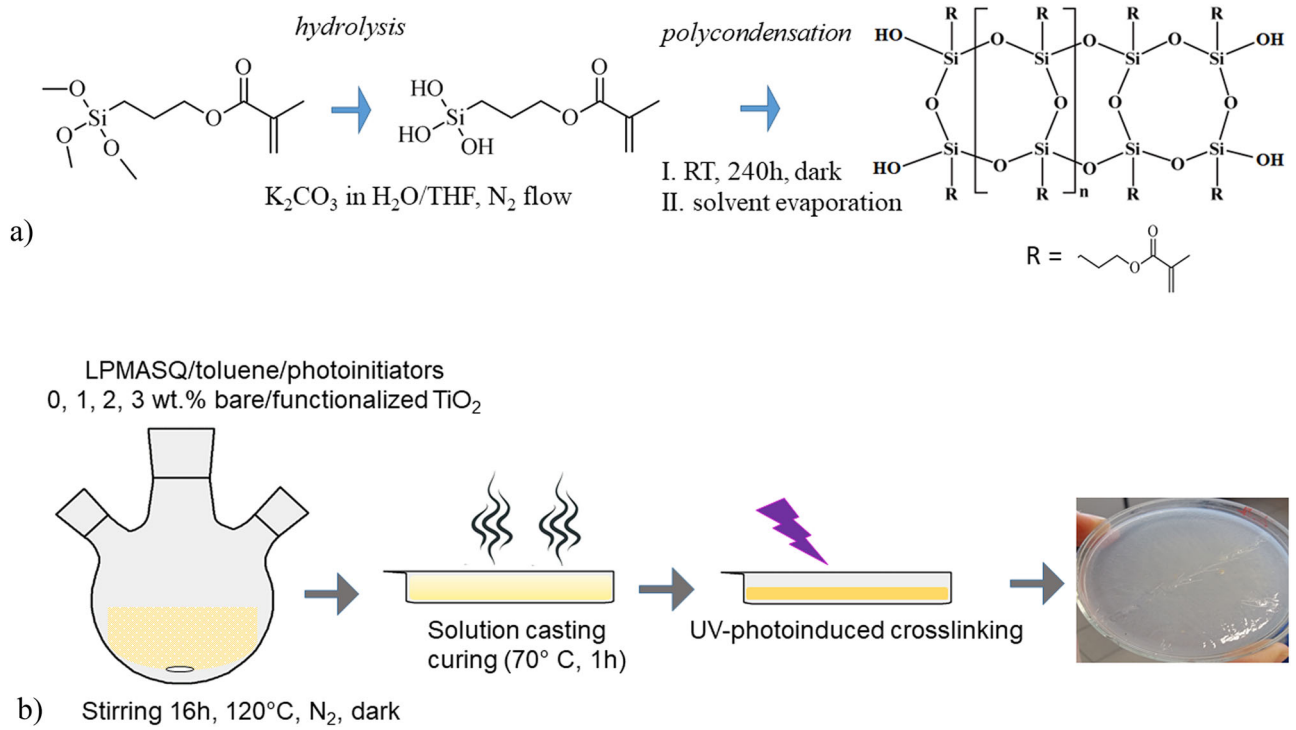

Scheme 1 **a** LPMASQ synthesis and (**b**) preparation of nanocomposites by solvent-casting and UV-induced photo-crosslinking

L_xfTiO2, where L represents the polymerized LPMASQ, and x is the wt% of TiO_2 and fTiO2 NPs.

2.3 Characterization techniques

Solid state NMR analyses were carried out with a Bruker 400WB spectrometer operating at a proton frequency of 400.13 MHz. Samples were packed in 4 mm zirconia rotors, which were spun at 8 kHz under air flow. Adamantane and Q_8M_8 were used as external secondary references. NMR spectra were acquired with cross polarization (CP) and single pulse (SP) sequences under the following conditions: ^{29}Si frequency: 79.48 MHz, contact time 5 ms, decoupling length 6.3 µs, recycle delay 10 s, 2k scans. Single pulse sequence: π/4 pulse 3.9 µs, recycle delay 60 s, 2k scans. ^{13}C frequency: 100.48 MHz, contact time 2 ms, decoupling length 5.9 µs, recycle delay 5 s, 2k scans. For variable contact time (VCT) experiments, the contact time has been varied from 0.05 to 9 ms with a spin-lock field strength equivalent to 63 kHz. To evaluate the cross-relaxation trends, the curves of the magnetization area as a function of CP contact time (t) are fitted with Eq. 1: [42]

$$M(t) = M0 \cdot e^{-t/T_{1\rho(H)}} \cdot \left(1 - e^{-t/T_{CH}}\right) \quad (1)$$

where M(t) is the peak area as a function of contact time t, M0 is the normalization constant, $T_{1\rho(H)}$ is the proton spin-lattice relaxation time in the rotating frame, and T_{CH} is the cross-polarization time constant. It is worth mentioning that multiexponential decays are also possible and could be explained in terms of the presence of different domains (i.e. homogeneity, segregation) [42, 43].

ATR-FTIR analyses were run in the 4000–550 cm^{-1} wavenumber range (64 scans, resolution 4 cm^{-1}), with a Varian 4100 Excalibur spectrometer equipped with a diamond ATR crystal.

XRD patterns were collected on polymerized LPMASQ and NCs with a Rigaku D/III max diffractometer (Rigaku), using Cu Kα$_1$ radiation (λ = 1.54056 Å) and a curved graphite monochromator in the diffracted beam, in the 2θ range 3°–80°, with sampling interval of 0.05°, and counting time of 2 s.

Thermogravimetric analysis was carried out on a Mettler Toledo TG50 with heating rate of 10 °C/min in N_2 atmosphere.

3 Results and discussion

The structural features of synthesized LPMASQ were studied by multinuclear NMR and FTIR experiments and results were compared with previous reports [10, 34, 36–38, 44]. ^{1}H and ^{13}C NMR (Online Resource Fig. S1a, b) spectra of the obtained sample show the typical signals of methacryloxypropyl groups and the absence of unreacted methoxy groups. The ^{29}Si NMR spectrum

(Fig. S1c) shows a broad, weak resonance in the region −52 to −58 ppm attributed to residual T^2 units (R-Si(OSi)$_2$OH, 9%), and the main complex resonance in the region −60 to −69 ppm due to T^3 units [10, 34, 44]. The FTIR spectrum (Online Resource Fig. S2) shows C–H stretching vibrations at 2943 and 2841 cm^{-1} due to methylene groups of the propyl chain; the signals related to Si-OH groups at 3500 and 960 cm^{-1} are not observable in the infrared spectrum, in agreement with the low amount of T^2 units in the ^{29}Si NMR spectrum. The strong absorption band at 1714 cm^{-1} and the signal at 1637 cm^{-1} are due respectively to C = O and C = C stretching vibrations of the methacryl groups. The appearance of two Si-O antisymmetric stretching vibrations at 1100 and 1020 cm^{-1} indicated the formation of dominant ladder-like structures [10, 34, 37, 44, 45], the high intensity of the absorption band at 1020 cm^{-1} points out lower structural regularity in comparison with LPMASQ produced by Lee et al. [36]. The thermogravimetric analysis (Online Resource Fig. S3) points out the remarkable thermal stability of synthesized LPMASQ according to the initial degradation temperature found at 375 °C and the shape of the thermal degradation curve is in agreement with those reported for ladder-like structures [31, 34, 36, 44]. FTIR, TG and NMR results overall confirm that the characteristics of the synthesized LPMASQ are similar to those previously reported [34, 36–38]. The slight lowering (5 °C) of the initial degradation temperature with respect to the value reported in [36] could be due to silanols, small defective structures, entrapped cycles or a slightly lower molecular weight of synthesized LPMASQ.

The effect of processing, namely solvent-casting and UV curing, on LPMASQ structure was investigated by means of solid state NMR, FTIR and XRD. The structural features of L sample (i.e. polymerized LPMASQ) evaluated by solid state NMR (Fig. 1) appear in agreement with previously published results [37, 38]. In the ^{13}C CPMAS spectrum (Fig. 1b), all the resonances of LPMASQ methacryloxypropyl chains are visible (labelling scheme in Fig. 1a), but both the strong reduction in intensity of the C = C related peaks (*e* and *g*) with respect to pristine LPMASQ (Online Resource Fig. S1) and the additional new peaks confirm the occurrence of radical polymerization [37], with partial conversion of the methacrylic double bond. As a matter of fact, signals appearing at 45 and 55 ppm (*g'* and *e'*, respectively) are related to the formation of new aliphatic carbons. Moreover, in the carbonyl region, a second C = O resonance (*d'*, 177 ppm) is also detected, which is downfield shifted with respect to the typical LPMASQ C = O peak (*d*, 165 ppm), and refers to the carbonyl close to methine *e'* and methylene *g'*.

The features of the inorganic skeleton of L sample were studied by silicon-29 NMR. LPMASQ backbone is characterized by fully condensed T^3 units (R-Si(OSi)$_3$) [36, 44], which produce in the ^{29}Si CPMAS spectrum (Fig. 1c) the asymmetric resonance at about −66 ppm. The amount of terminal T^2 units (δ -57 ppm, ≈7%) decreases slightly compared to as-synthesized LPMASQ; this result is to be expected considering that the solvent casting step followed by thermal curing at 70 °C allow some condensation of residual silanols. The T^3 band is centered at −67 ppm and its asymmetric shape results from the overlapping of the resonances detected in the ^{29}Si NMR spectrum of pristine LPMASQ (Online Resource Fig. S1c) related to T^3 units in different conformations [45]. The components linewidth (LW) helps to discriminate among the different conformations assumed by the LPMASQ chains, since it is known that the LW of the T^3 peak is a measure of the regularity of the polymer skeleton [44–46]. Accordingly, sharp signals with LW below 200 Hz indicate highly ordered and long ladder chains. Thus, following the literature, the observed T^3 resonance could be described as a main component (δ -67.1 ppm), representing the completely condensed linear ladders. The downfield and upfield shoulders could then be attributed to ladder-type silsesquioxane chains forming rigid stacks by folding together, short oligomers and defective structures similar to open cages, respectively [8, 44–51].

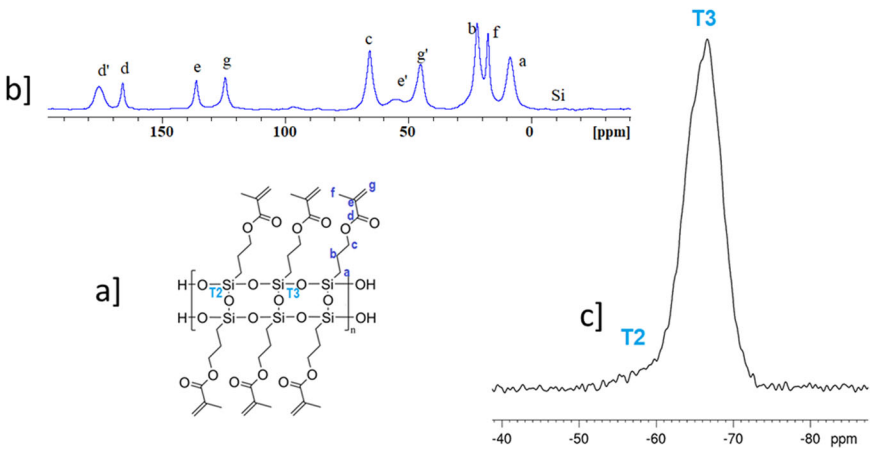

Fig. 1 LPMASQ structural scheme and carbon labelling (**a**), ^{13}C (**b**) and ^{29}Si (**c**) CPMAS NMR spectra of L sample

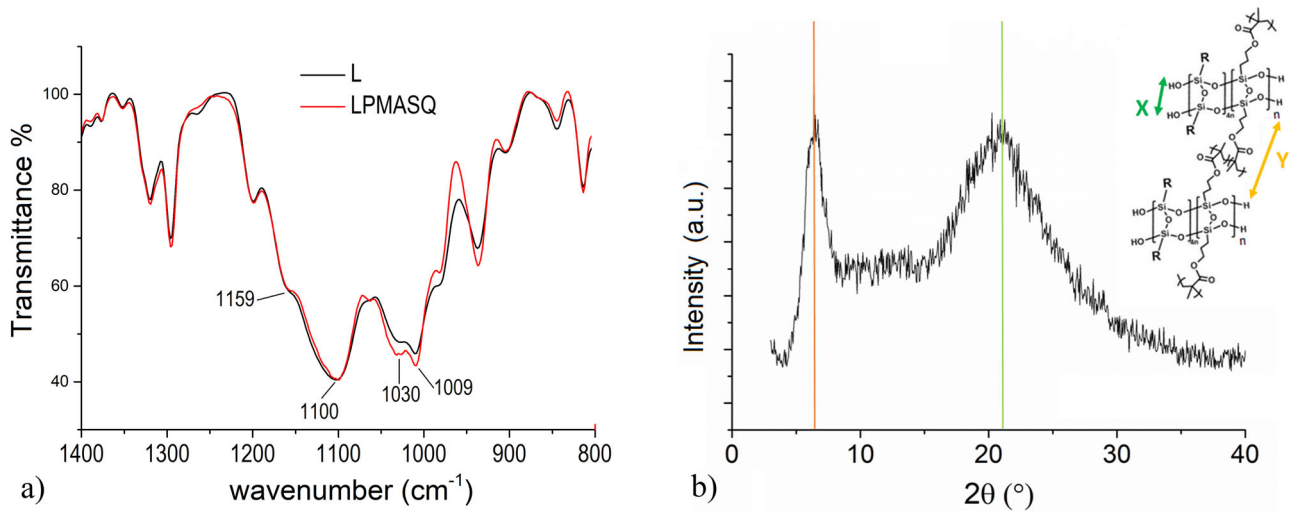

Fig. 2 **a** Si-O antisymmetric stretching region in the ATR-FTIR spectra of pristine LPMASQ and L samples (**b**) XRD pattern of L, with the structural scheme showing X and Y distances

The analysis of the FTIR spectra recorded on LPMASQ and sample L (Fig. 2a) strengthens the assignment of T^3 components in the NMR spectrum, while showing that the structural features of polymerized sample are not substantially modified with respect to LPMASQ. As a matter of fact, the siloxane stretching bands of L and LPMASQ are almost identical, supporting the use of pristine LPMASQ T^3 components in the line-shape analysis of polymerized samples. The Si-O antisymmetric stretching vibrations produce a band in the range 1200–900 cm^{-1}, which is the result of overlapping of various components. In detail, the shoulder at 1159 cm^{-1} is correlated to T_7OH_3 or T_8OH_2 open cage structures, the signal at 1100 cm^{-1} is attributed to cage-like architectures probably due to chain folding of LPSQs, and the components at 1030 and 1009 cm^{-1} are assigned to linear ladder-type units of different length [44, 45, 47].

The relative intensity of the two bands centered at 1100 and 1020 cm^{-1} appears almost unchanged, in agreement with the limited secondary condensation shown by ^{29}Si NMR. FTIR shows that minor changes occurred and the ladder-like network overall maintains the structural features of the starting LPMASQ [52].

Finally, the diffraction pattern of L (Fig. 2b) is characterized by two amorphous halos, respectively, centred at $2\theta \sim 6°$, associated with the intramolecular periodic chain-to-chain distance (denoted as Y in inset of Fig. 2b) and at $2\theta \sim 20°$, associated with the average thickness X of the Si–O–Si silsesquioxane structure [38, 44]. In addition, a third very broad hump centred at $2\theta \sim 11°$ can be detected. This component has been previously observed in LPMASQ/silica NCs prepared by photopolymerization [38], and is attributed to the distances (Y') produced by the side chains polymerization, which can lead to a broad distribution of intramolecular chain-to-chain distances as a result of variable side-chain lengths [53].

The NCs, obtained by solution casting and photopolymerization, appear as quasi-transparent homogeneous films that can easily be detached from the substrate. SEM analysis reveals that all samples are characterized by a typical surface waviness, but no defects are detected at low magnification (Online Resource Fig. S6); however, the EDX analysis pointed out that even if TiO_2 is distributed throughout the samples, some aggregates are present regardless of NPs surface modification [39]. The functionalization of titania particles with MPTMS was confirmed by FTIR analysis (Fig. S5); the fTiO2 spectrum presents bands at 1716 and 1635 cm^{-1} due to methacryloxy groups and broad, weak Si-O antisymmetric stretching bands in the range 1200 to 1000 cm^{-1}. The amount of grafted molecules was evaluated by TG analysis through the net weight loss in the range 150 to 1000 °C (2.8%) [39].

Despite the low amount (up to 3%w), the addition of both bare and functionalized TiO_2 NPs to LPMASQ clearly affects the polymerization of methacryloxypropyl chains. As a matter of fact, the ^{13}C CPMAS spectra (Fig. 3) show both a slight sharpening (the linewidth difference is about 20%) of the LPMASQ signals and the decrease in area of *d'*, *e'* and *g'* resonances compared to L. Surprisingly, *g* resonance displays both a relevant linewidth decrease and an intensity increase with increasing the TiO_2 loading, but at the moment there is not a clear explanation for these phenomena. It should be mentioned that in the case of L_xfTiO2 samples, it is not possible to distinguish the features of LPMASQ side chains and titania surface

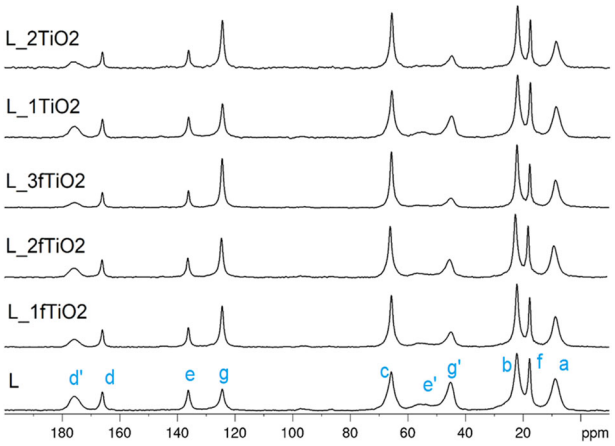

Fig. 3 ^{13}C CPMAS spectra (contact time: 2 ms) of L, L_xTiO_2 and L_xfTiO2 NCs

Table 1 Integration of the carbonyl region of the ^{13}C CPMAS NMR spectra shown in Fig. 3. The relative area of d' with respect to the sum d+d' gives the extent of LPMASQ polymerization

	%d' ± 0.6		%d' ± 0.6
δ (ppm)	177.3		177.3
L	66.3	L_1fTiO2	56.4
L_1TiO2	64.2	L_2fTiO2	56.2
L_2TiO2	53.0	L_3fTiO2	49.9

functions, due to the identical molecular structure and the low amount of MPTMS grafted onto the NPs.

To quantify the methacrylic double bond conversion, the % of *d'* is calculated from the relative areas of *d* and *d'* peaks. The values of Table 1 show that the extent of polymerization decreases with increasing titania amount, but a clear dependence on NPs functionalization cannot be argued.

In LPMASQ/silica NCs prepared by photopolymerization [38] we observed a similar reduction of methacrylic double bond conversion, which can be explained by the decrease of energy available for polymerization reactions due to the capability of inorganic particles to absorb or scatter light [54].

The organization of LPMASQ ribbons is also affected by NP addition, according to the changes observed for the inorganic backbone in ^{29}Si spectra (Fig. 4).

Similarly to what was noticed for the ^{13}C resonances, a narrowing of the T^3 peak is observable in LPMASQ/titania NCs, as the full width at half maximum (FWHM) is about 360 Hz compared with the observed value of 449 Hz for L sample. It is worth noting that, while the signal still exhibits evident asymmetry, it appears that the downfield components gradually reduce upon TiO_2 addition.

These observations can be deepened by applying a profile fitting of T^3 peaks. The line-shape analysis is performed

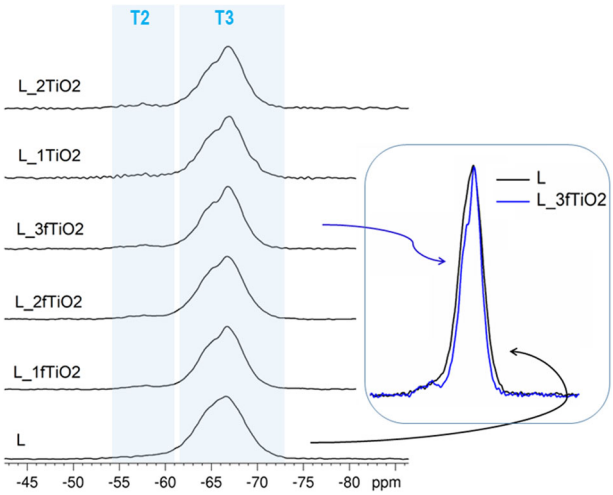

Fig. 4 ^{29}Si CPMAS NMR spectra of the LPMASQ/titania samples; the superposition of two ^{29}Si spectra is shown in the inset to highlight the variation of the lineshape

directly on CPMAS spectra, since the comparison between CPMAS and MAS results (Online Resource Fig. S7) indicates that the spectra are completely superimposable and CPMAS spectra present higher S/N ratio. In all samples, the T^3 resonance can be successfully fitted with five components, according to the above reported discussion for pure L sample. The results, summarized in Table S1 (Online Resource), point out that the relative amount of the different components is related to TiO_2 loading. Only the component at δ -67.1 ppm appears to grow with the TiO_2 amount at the expenses of the others (i.e. δ −68.7, −65.3, −64.1 and −62.8 ppm) that slightly decrease or remain constant, causing the observed signal asymmetry. NMR results are in agreement with previously reported FTIR evidence, which pointed out slight differences of the siloxane components in the Si-O antisymmetric stretching vibration band, in particular the decrease in intensity of the peaks at 1105 and 1067 cm^{-1} respectively assigned to cage-like structures due to chains folding and defective open cage structures [39]. Combining this information and the literature reports [8, 44–51], the components could be assigned as follows: δ -67.1 ppm is due to long linear ladders, the upfield component at −68.7 ppm to defective structures similar to open cages, and the three downfield components at −64.1 ppm to folded ladder chains and −62.8/−65.3 ppm to low molecular weight structures.

According to ^{13}C NMR results, TiO_2 negatively affects the extent of LPMASQ polymerization; thus, the increase of the linear component with titania load could be correlated with the lower methacrylic double bond conversion observed in LPMASQ/titania NCs. To validate this hypothesis, in Fig. 5 the intensity of the different T^3 silicon resonances obtained from the corresponding ^{29}Si NMR spectra (Online Resource Table S1) are reported as a

function of the extent of polymerization calculated from the carbon-13 spectra (Table 1).

The component at -67.1 ppm due to long linear ladders rises with the decrease of methacrylic double bond polymerization, while the other T^3 components slightly reduce or remain constant, confirming that TiO_2 not only negatively affects the polymerization process, but also influences the distribution of ladders' conformations. Figure 6 summarises the structural effects pointed out by ^{13}C and ^{29}Si NMR studies.

Finally, the comparison between L sample and nanocomposites reveals that the amount of T^2 units (Online Resource Table S1) remains constant (≈7%) in the samples produced with fTiO2. The T^2/T^3 ratio, conversely, decreases slightly (5.5%) with the use of bare TiO_2 suggesting that condensation between Ti-OH groups and silanols may have occurred during solvent-casting and thermal curing steps.

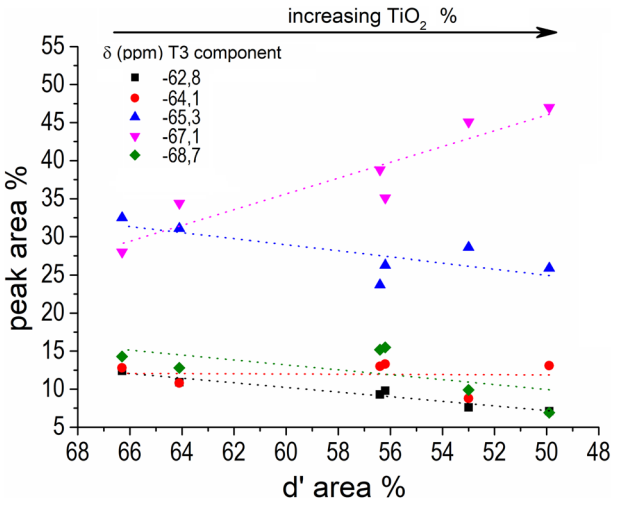

Fig. 5 Correlation plot between the amount of T^3 components (peak area % from Table S1) and the extent of methacrylic double bond polymerization expressed as the d' relative area (% of the whole C = O signals from Table 1). Symbols and colours identify the specific T^3 component; dotted lines are linear tendency curves

This reactivity contributes to the complexity of both NCs structure and hybrid interface, since few siloxane ribbons can also be directly bonded to the TiO_2 surface in addition to possible copolymerization of methacrylate groups of LPMASQ and grafted MPTMS.

On the other hand, the secondary condensation of LPMASQ silanols, also observed in sample L, could preferentially involve small and defective mobile fragments and together with the unfolding of the folded ladder structures supports the increase in linear ladders.

Since the results show that LPMASQ polymerization is controlled by the amount of TiO_2 NPs regardless of functionalization, the study of molecular dynamics of organic side-chains in the slow (kHz) regime through ^{13}C NMR was addressed to shed light on the filler-matrix interactions in NCs produced with bare and functionalized titania [55–57]. To fulfil this aspect, the evolution of the magnetization (i.e. the peak area) of L, L_2fTiO2 and L_2TiO2, as representative samples, has been followed as a function of the contact time in ^{13}C CP experiments (Fig. 7a shows the trend for all of the carbon atoms of sample L). VCT curves are governed by kinetics and dynamics of the process of cross-polarization from protons to carbons and may be fitted through different models [43]. The rapid increase in the curves at short time intervals is dominated by ^{1}H-^{13}C polarization transfer (T_{CH}). T_{CH} values depend on the mutual C–H distance and H atoms' density in the proximity of a given C atom (ms range) but are affected by the group mobility that interferes with ^{1}H-^{13}C polarization transfer [58]. After the maximum, the curve decay is governed mainly by the spin-lattice relaxation in the rotating frame $T_{1\rho(H)}$. The decay constant $T_{1\rho(H)}$ of the protons is a volume property averaged over a distance of ca. 2 nm and provides information on the relative mobility of the H atoms. In homopolymers, high $T_{1\rho(H)}$ values are related to long chains or rigid/crystalline materials and low values are associated with small molecules/domains and the presence of amorphous phases [42, 43]. Moreover, $T_{1\rho(H)}$ provides information on possible regions of morphological heterogeneity.

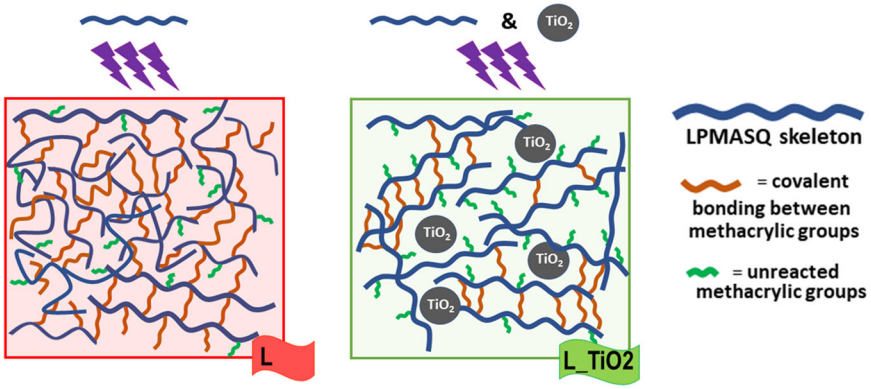

Fig. 6 Addition of titania in polymerized LPMASQ leads to the decrease of methacrylic group polymerization and the increase of linear ladders

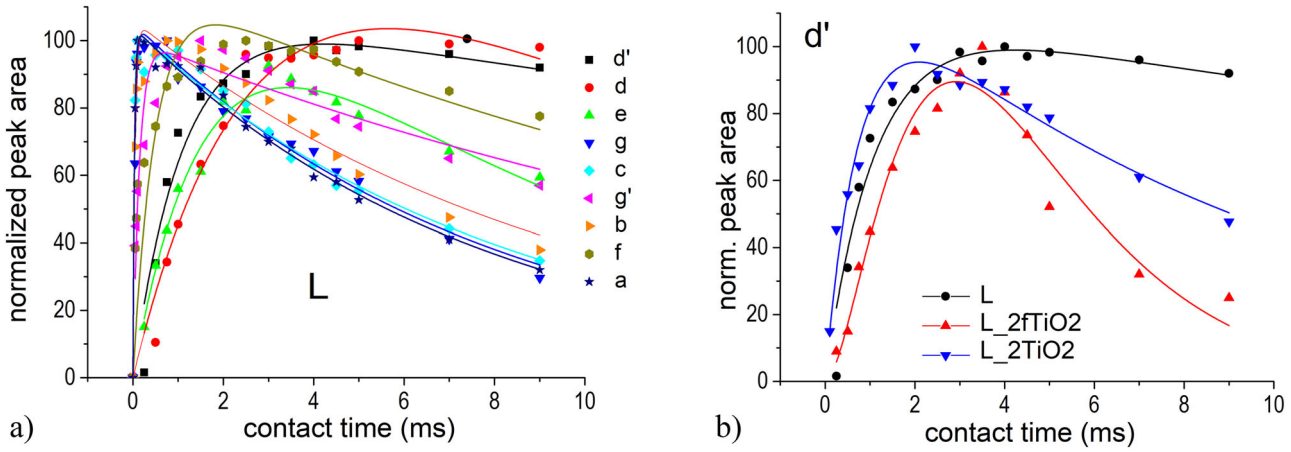

Fig. 7 ^{13}C VCT curves (**a**) of all the resonances in sample L and (**b**) of signal *d'* in the samples L, L_2fTiO2 and L_2TiO2

Involving a large number of monomeric units, $T_{1\rho(H)}$ can be significantly affected by the spin diffusion process, which tends to average it to a single mean value in polymeric chains [55, 57].

In this work, the magnetization curves of LPMASQ carbons were normalized to have the maximum intensity equal to 100 and the curves were obtained by fitting with Eq. 1, in order to highlight the different behavior of all functional groups. The carbons in sample L clearly present different trends (Fig. 7a). The curve growth, which is described by T_{CH} constant, is characterized by different slopes, depending on the dipolar coupling strength, typical of each functional group. Interestingly, looking at the decay part of the curves expressed by the parameter $T_{1\rho(H)}$, relevant differences among the functional groups can be appreciated that indicate inefficient spin diffusion at RT. Voelkel [43] explained this phenomenon with a high molecular mobility of the system, which averages out the proton-proton dipolar interaction. In our case, this hypothesis can be considered viable, taking into account the narrow signal linewidths (200–300 Hz) observed in the ^{1}H MAS NMR spectrum of sample L (Online Resource Fig. S8) [43, 56].

Similar considerations can be made by comparing the curves of functional groups in LPMASQ/TiO_2 NCs. However, the comparison of trends of the same functional group in samples prepared with and without titania highlights different behaviors. Among the functional groups, the most interesting information is obtained from the study of the carbonyl groups, which are the most sensitive to the presence of the filler. Indeed, we have shown above that it is possible to derive information about the polymerization process from the analysis of carbonyl carbons in unreacted and polymerized methacrylate groups, respectively. In addition, the carbonyl carbons are of particular interest also for the study of molecular dynamics, since they are not directly linked to H and the nearest protons are responsible for their relaxation in the rotating frame, providing useful information on the chains' overall behaviour [55, 56]. Both growth and decay of *d'* curves (Fig. 7b) are very sensitive either to the presence of NPs and their surface functionalization. In particular, the *d'* curve relaxes faster for L_2TiO2 and even more in the case of L_2fTiO2. Thus, the presence of TiO_2 and fTiO2 seems to differently influence the folding/organization of the LPMASQ chains during the photopolymerization process. The NPs probably induce a different arrangement of LPMASQ polymerized side-chains, and the functionalization of the particles' surfaces enhances this effect. The dynamics of *d'* appear to be sensitive to the chemical groups present on the NPs surface. As a consequence, the different surface features, i.e. titanols available for H-bonding or methacrylic groups able to copolymerize, induce conformation rearrangements favouring less ordered chain packing [53, 57], in agreement with the ^{29}Si results.

The curves of carbonyl *d* (Online Resource Fig. S9) show similar growths, but the different slope of L_2fTiO2 curve suggests higher mobility of the close protons; the decay appears slightly faster for the composites than for L, generally suggesting moderate sensitivity of unreacted chains to the presence of NPs. The different behaviour of *d* and *d'* is highlighted by the comparison of the curves in all the three samples. Interestingly, similar, though less obvious, trends are found for the closest *g'* and *g* carbons (Online Resource Fig. S9). Finally, the propyl carbons *a*, *b* and *c* have fairly similar trends and do not appear sensitive to the presence of filler, due to its vicinity to the LPMASQ inorganic skeleton.

From these results, both organization and dynamics of polymerized side-chains appear strongly affected by NPs and even more by their surface functionalization, while the effect is less pronounced for resonances belonging to

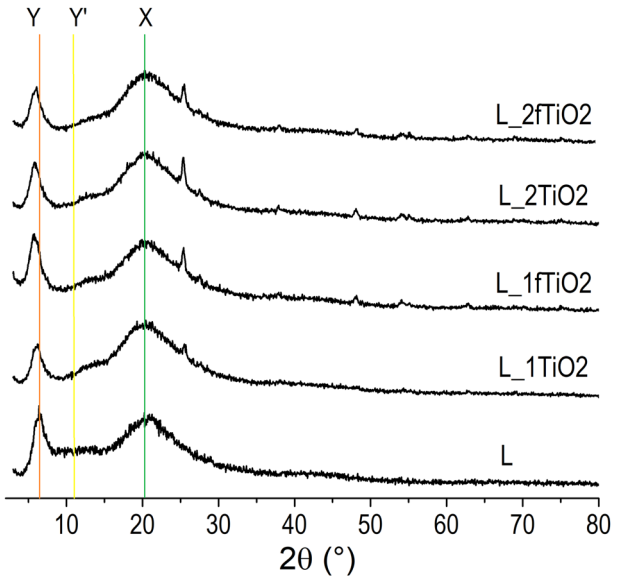

Fig. 8 XRD patterns of L and NCs with bare and functionalized TiO_2

unreacted LPMASQ side-chains. Polymer chains suffer structural deformation in close proximity to surfaces, with typically a reduction of the free volume moving away from the NP surface to the bulk, reflected in a chain density variation [59]. Therefore, an alteration in polymer chain organization near the interfaces is possible with respect to the bulk region.

To investigate the effects induced by NP addition at a different length scale and complement the information obtained by NMR at the molecular level, the XRD patterns of L and selected NCs were compared (Fig. 8).

In L_xTiO2 and L_xfTiO2 samples, sharp peaks account for the presence of different amounts of titania (anatase, PDF 21-1272, rutile PDF 21-1276, in agreement with the presence of both anatase and rutile phases in Aeroxide P25 [60]). These reflections are overlapped with the amorphous halos observed in L sample. The peak related to periodic intramolecular chain-to-chain distance Y moves to lower angles with the addition of titania, while the signal related to the siloxane backbone thickness X appears unchanged. Moreover, the third halo (related to distance Y') that was observed at $2\theta \sim 11°$ in sample L, becomes narrower and shifts towards higher angles (Online Resource Fig. S10), as a consequence of the different polymerized side-chain arrangement highlighted by solid state NMR.

The profile fitting analysis of XRD patterns of selected samples (Online Resource Fig. S11) was run in order to quantify the observed changes. Table 2 reports the calculated d-spacing values and the corresponding FWHM for the three reflections, and the parameter R, defined as the ratio of intensities of Y and X related signals, which gives information on structural regularity and concentration of defects in ladder polysilsesquioxane [61]. The constant X

Table 2 Results of the profile fitting analysis of XRD patterns of L, L_1fTiO2 and L_2fTiO2

Sample	d_Y, nm (FWHM,°)	$d_{Y'}$, nm (FWHM,°)	d_X, nm (FWHM,°)	R (I_Y/I_X)
L	1.40 (1.8)	0.98 (9)	0.44 (8.7)	0.92
L_1fTiO2	1.52 (1.59)	0.69 (2.0)	0.44 (8.9)	0.87
L_2fTiO2	1.51 (1.68)	0.67 (3.5)	0.44 (9.0)	0.64

value equal to 0.44 nm is comparable to reported distances in ladder silsesquioxanes and confirms that the siloxane backbone is unaffected by the addition of NPs, as also proved by the unmodified FWHM. The intramolecular chain-to-chain distance Y increases in NCs, but the results do not suggest a clear trend with the amount and functionalization of nanoparticles. TiO_2 addition strongly modifies the third halo, which is likely to be related to the polymerization process and consequently to organic side-chains distances.

Accordingly, sample L presents a very broad distribution of such distances as a consequence of random polymerization among LPMASQ propylmethacrylate chains. In NCs, TiO_2 addition reduces the distribution of side-chain distances, which become shorter with respect to the case of sample L. This result, together with the observed increase of Y distance and the related signal narrowing, suggests a separation between domains characterized respectively by long ordered and short disordered organic side-chains [53]. This hypothesis is strengthened by the large decrease of R value in NCs, which points out a relevant increase of defects with loss of the structural regularity of ladders.

4 Conclusions

The effect of photopolymerization and addition of a small percentages of TiO_2 nanoparticles, both bare and functionalized, on ladder-like poly(methacryloxypropyl) silsesquioxanes was studied by combining solid-state NMR and X-ray diffraction to highlight structural changes at different length scales.

Adding up to 3 wt.% of titania nanoparticles reduces the methacrylate double bond polymerization and changes the distribution of ladders structures, according to ^{13}C and ^{29}Si solid state NMR. In particular, the decrease of the extent of organic side-chain polymerization can be correlated with the increase of linear long ladders, pointing out the effect of TiO_2 both on the polymerization ability and the chain conformation of LPMASQ.

The XRD study of the polymerized LPMASQ (L) sample highlights the appearance of a broad distribution of distances Y' produced by the random polymerization among propylmethacrylate chains, leading to a wide distribution of ladder chain-to-chain distances. This reflection adds to the characteristic amorphous halos due to the typical LPSQ intramolecular chain-to-chain distance Y and the length of the siloxane backbone X. The addition of titania nanoparticles, regardless of functionalization, results in an increase in distance Y and the narrowing of the distribution of Y' distances, which become shorter. Moreover, the decrease of the parameter R highlights the loss of the ladders' structural regularity.

Interestingly, the effect induced by the use of functionalized NPs is revealed by approaching the study of the organic chains' molecular dynamics in the slow regime, here probed through the analysis of cross-polarization kinetics. Above all, this pointed out that the polymerized organic chains display a change of conformations/folding as a result of changing interactions at the filler-polymer interface.

In summary, this study, beyond demonstrating that even the incorporation of very low loadings of TiO_2 NPs produce relevant modifications on the architecture of ladder-like silsesquioxanes, constitutes a methodological approach that can be extended also to other composite systems, opening the possibility to better understand and tune their structural and interfacial properties with positive implications on the functional properties.

Acknowledgements The authors warmly acknowledge Dr. F. Babonneau for the helpful discussions about NMR data.

Funding Open access funding provided by Università degli Studi di Trento within the CRUI-CARE Agreement.

Compliance with ethical standards

Conflict of interest The authors declare no competing interests.

References

1. Ayandele E, Sarkar B, Alexandridis P (2012) Polyhedral oligomeric silsesquioxane (poss)-containing polymer nanocomposites. Nanomaterials 2:445–475
2. Raftopoulos KN, Pielichowski K (2016) Segmental dynamics in hybrid polymer/POSS nanomaterials. Prog Polym Sci 52:136–187
3. Kuo SW (2016) Building blocks precisely from polyhedral oligomeric silsesquioxane nanoparticles. ACS Cent Sci 2:62–64
4. Kuo SW, Chang FC (2011) POSS related polymer nanocomposites. Prog Polym Sci 36:1649–1696
5. Fina A, Monticelli O, Camino G (2010) POSS-based hybrids by melt/reactive blending. J Mater Chem 20:9297–9305
6. Ren Z, Yan S (2016) Polysiloxanes for optoelectronic applications. Prog Mater Sci 83:383–416
7. Lee AS, Choi SS, Baek KY, Hwang SS (2016) Hydrolysis kinetics of a sol-gel equilibrium yielding ladder-like polysilsesquioxanes. Inorg Chem Commun 73:7–11
8. Kaneko Y, Toyodome H, Shoiriki M, Iyi N (2012) Preparation of ionic silsesquioxanes with regular structures and their hybridization. Int J Polym Sci 2012:684278
9. Rathnayake H, White J, Dawood S (2021) Polysilsesquioxane-based organic-inorganic hybrid nanomaterials and their applications towards organic photovoltaics. Synth Met 273:116705
10. Dirè S, Borovin E, Ribot F (2018) Architecture of silsesquioxanes. In: Klein L, Aparicio M, Jitianu A (eds) Handbook of Sol-Gel Science and Technology. Springer, Cham
11. Tanaka K, Chujo Y (2012) Advanced functional materials based on polyhedral oligomeric silsesquioxane (POSS). J Mater Chem 22:1733–1750
12. Goffin AL, Duquesne E, Raquez E, Miltner M, Ke X, Alexandre M, Van Tendeloo G, Van Mele G, Dubois P (2010) From polyester grafting onto POSS nanocage by ring-opening polymerization to high performance polyester/POSS nanocomposites. J Mater Chem 20:9415–9625
13. Zhou HI, Ye Q, Xu J (2017) Polyhedral oligomeric silsesquioxane-based hybrid materials and their applications. Mater Chem Front 1:212–230
14. Hwang SH, Lee JY, Lee JH (2019) Effect of the silsesquioxane structure on the mechanical properties of the silsesquioxane-reinforced polymer composite films. Prog Org Coat 137:105316
15. Jo YY, Lee AS, Baek KY, Lee H, Hwang SS (2017) Thermally reversible self-healing polysilsesquioxane structure-property relationships based on Diels-Alder chemistry. Polymer 108:58–65
16. Kowalewska A, Nowacka M, Makowski T, Michalski A (2016) Thermal stability of self-assembled surfaces and micropatterns made of ladder polysilsesquioxanes. Polymer 90:147–155
17. Kowalewska A, Herc AS, Bojda J, Palusiak M, Markiewicz E, Ławniczak P, Nowacka M, Sołtysiak J, Różański A, Piorkowska E (2021) Supramolecular interactions involving fluoroaryl groups in hybrid blends of polylactide and ladder polysilsesquioxanes. Polym Test 94:107033
18. Hwang SO, Lee AS, Lee YJ, Park SH, Jung KI, Jung HW, Lee JH (2018) Mechanical properties of ladder-like polysilsesquioxane-based hard coating films containing different organic functional groups. Prog Org Coat 121:105–111
19. Lee AS, Jo YY, Jeon H, Choi SS, Baek KY, Hwang SS (2015) Mechanical properties of thiol-ene UV-curable thermoplastic polysilsesquioxanes. Polymer 68:140–146
20. Jo YY, Lee AS, Baek KY, Lee H, Hwang SS (2017) Multi-crosslinkable self-healing polysilsesquioxanes for the smart recovery of anti-scratch properties. Polymer 124:78–87
21. Kickelbick G (2007) Introduction to hybrid materials. In: Kickelbick G (ed) Hybrid materials. Synthesis, characterization, and applications. Wiley, Weinheim

22. Choi YM, Jung J, Lee AS, Hwang SS (2021) Photosensitive hybrid polysilsesquioxanes for etching-free processing of flexible copper clad laminate. Compos Sci Technol 201:108556
23. Herc AS, Lewiński P, Kaźmierski S, Bojda J, Kowalewska A (2020) Hybrid SC-polylactide/poly(silsesquioxane) blends of improved thermal stability. Thermochim Acta 87:178592
24. Herc AS, Bojda J, Nowacka M, Lewiński P, Maniukiewicz W, Piorkowska E, Kowalewska A (2020) Crystallization, structure and properties of polylactide/ladder poly(silsesquioxane) blends. Polymer 201:122563
25. Nowacka M, Fischer C, Kowalewska A, Hebda M, Hodor K (2017) Thermally induced phenomena leading to degradation of poly(silsesquioxane) materials. Eur Pol J 86:17–28
26. Gao Q, Qi S, Wu Z, Wu D, Yang W (2011) Synthesis and characterization of functional ladder-like polysilsesquioxane and their hybrid films with polyimide. Thin Solid Films 519:6499–6507
27. Zhang L, Tian G, Wang X, Qi S, Wu Z, Wu D (2014) Polyimide/ladder-like polysilsesquioxane hybrid films: Mechanical performance, microstructure and phase separation behaviors. Compos Part B: Eng 56:808–814
28. Oh H, Jo E, Jang HW, Jung H, Park SH, Kim AY, Jung JH, Youk JH, Lee M (2022) Hard coating films of fluorine-containing ladder-like structured polysilsesquioxane as negative triboelectric materials for high-performance triboelectric generators. Extrem Mech Lett 50:101533
29. Wang Q, Zhang H, Cui Z, Zhou Q, Shangguan X, Tian S, Zhou X, Cui G (2019) Siloxane-based polymer electrolytes for solid-state lithium batteries. Energy Storage Mater 23:466–490
30. Choi MH, Seo JY, Ahn J, Woo HJ, Cho S, Hwang SS, Lee AS, Baek KY (2021) Flowable polysilsesquioxanes as robust solvent-free optical hard coatings. React Funct Polym 167:105030
31. Prado LAS, De A, Radovanovic E, Pastore HO, Yoshida IVP, Torriani IL (2000) Poly(phenylsilsesquioxane)s: structural and morphological characterization. J Polym Sci Part A: Polym Chem 38:1580–1589
32. Zhang ZX, Hao J, Xie P, Zhang X, Han CC, Zhang R (2008) A well-defined ladder polyphenylsilsesquioxane (Ph-LPSQ) synthesized via a new three-step approach: monomer self-organization−lyophilization surface-confined polycondensation. Chem Mater 20:1322–1330
33. Lee S, Choi SS, Lee HS, Baek KY, Hwang SS (2010) High photo- and electroluminescence efficiencies of ladder-like structured polysilsesquioxane with carbazole groups. J Mater Chem 20:9852–9854
34. Choi SS, Lee S, Lee HS, Baek KY, Hwang SS (2011) Synthesis and characterization of UV-curable ladder-like polysilsesquioxane. J Polym Sci Part A: Polym Chem 49:5012–5018
35. Lee S, Choi SS, Lee HS, Baek KY, Hwang SS (2012) A new, higher yielding synthetic route towards dodecaphenyl cage silsesquioxanes: synthesis and mechanistic insights. Dalton Trans 41:10585–10588
36. Lee SS, Lee JH, Lee J, Hwang SM, Min Koo C (2014) Novel polysilsesquioxane hybrid polymer electrolytes for lithium ion batteries. J Mater Chem A 2:1277–1283
37. D'Arienzo M, Dirè S, Masneri V, Rovera D, Di Credico B, Callone E, Mascotto S, Pegoretti A, Ziarelli F, Scotti R (2018) Tailoring the dielectric and mechanical properties of polybutadiene nanocomposites by using designed ladder-like polysilsesquioxanes. ACS Appl Nano Mater 1:3817–3828
38. D'Arienzo M, Dirè S, Cobani E, Orsini S, Di Credico B, Antonini C, Callone E, Parrino F, Dalle Vacche S, Trusiano G, Bongiovanni R, Scotti R (2020) SiO2/Ladder-like polysilsesquioxanes nanocomposite coatings: playing with the hybrid interface for tuning thermal properties and wettability. Coatings 10:913
39. Parrino F, D'Arienzo M, Callone E, Conta R, Di Credico B, Mascotto S, Meyer A, Scotti R, Dirè S (2021) TiO_2 containing hybrid nanocomposites with active–passive oxygen scavenging capability. Chem Eng J 417:129135
40. Ingrosso C, Esposito Corcione C, Striani R, Comparelli R, Striccoli M, Agostiano A, Curri ML, Frigione M (2015) UV-curable nanocomposite based on methacrylic-siloxane resin and surface-modified tio2 nanocrystals. ACS Appl Mater Interfaces 7:15494–15505
41. Liska R (2011) Industrial photoinitiators: a technical guide. by W. Arthur Green. Chem Phys Chem 12:1389–1389
42. Kolodziejski W, Klinowski J (2002) Kinetics of cross-polarization in solid-state NMR: a guide for chemists. Chem Rev 102:613–628
43. Voelkel R (1988) High-resolution solid-state 13C-NMR spectroscopy of polymers. Angew Chem Int Ed Engl 27:1468–1483
44. Choi SS, Lee AS, Hwang SS, Baek KY (2015) Structural control of fully condensed polysilsesquioxanes: ladderlike vs cage structured polyphenylsilsesquioxanes. Macromolecules 48:6063–6070
45. Borovin E, Callone E, Papendorf B, Guella G, Diré S (2016) Influence of sol–gel conditions on the growth of thiol-functionalized silsesquioxanes prepared by in situ water production. J Nanosci Nanotechnol 16:3030–3038
46. Seki H, Kajiwara T, Abe Y, Gunji T (2010) Synthesis and structure of ladder polymethylsilsesquioxanes form sila-functionalized cyclotetrasiloxanes. J Organomet Chem 695:1363–1369
47. Borovin E, Callone E, Ribot F, Diré S (2016) Mechanism and kinetics of oligosilsesquioxane growth in the in situ water production sol–gel route: dependence on water availability. Eur J Inorg Chem 2166–2174.
48. Abe Y, Gunji T (2004) Oligo- and polysiloxanes. Prog Polym Sci 29:149–182
49. Petrova IM, Buryak AK, Peregudov AS, Strelkova TV, Kononova EG, Bushmarinova IS, Makarova NN (2015) Effect of stereoisomerism of (tetrahydroxy)(tetraphenyl) cyclotetrasiloxanes on the siloxane framework in polyphenylsilsesquioxanes obtained by polycondensation in the presence of layered-architecture compounds. Mendeleev Commun 25:229–231
50. Suyama K, Gunji T, Arimitsu K, Abe Y (2006) Synthesis and structure of ladder oligosilsesquioxanes: tricyclic ladder oligomethylsilsesquioxanes. Organometallics 25:5587–5593
51. Sato Y, Hayami R, Gunji T (2022) Characterization of NMR, IR, and Raman spectra for siloxanes and silsesquioxanes: a mini review. J Solgel Sci Technol 104:36–52
52. Park ES, Ro HW, Nguyen CV, Jaffe RL, Yoon DY (2008) Infrared spectroscopy study of microstructures of poly(-silsesquioxane)s. Chem Mater 20:1548–1554
53. Zhang L, Dai D, Zhang R (1997) The synthesis and x-ray diffraction study of the ladder-like polysilsesquioxanes with side-chain ester groups. Polym Adv Technol 8:662–665
54. Azan V, Lecamp L, Lebaudy P, Bunel C (2007) Simulation of the photopolymerization gradient inside a pigmented coating: Influence of TiO_2 concentration on the gradient. Prog Org Coat 58(1):70–75
55. DaSilva EP, Tavares MIB (1998) Solid state nmr study of poly(methyl methacrylate)/polyvinylpyrrolidone blends. Pol Bull 41:307–310
56. Phinnyocheep P, Saelao J, Buzarè JY (2007) Mechanical properties, morphology and molecular characteristics of poly(ethylene terephthalate) toughened by natural rubber. Polymer 48:5702–5712
57. Spinella A, Bondioli F, Nasillo G, Renda V, Caponetti E, Messori M, Morselli D (2017) Organic-inorganic nanocomposites prepared by reactive suspension method: investigation on filler/matrix interactions and their effect on the nanoparticles dispersion. Colloid Polym Sci 295:695–701
58. Benard F, Buzaré JY, Campistron I, Laguerre A, Lavald F (2007) Influence of silica fillers during the electron irradiation of DGEBA/TETA epoxy resins, part III: solid-state NMR investigations. Polym Degrad Stab 92:785–794

59. Feng J, Venna SR, Hopkinson DP (2016) Interactions at the interface of polymer matrix-filler particle composites. Polymer 103:189–195
60. Jianga X, Manawanb M, Fengc T, Qiana R, Zhaoa T, Zhoua G, Kongd F, Wange Q, Daia S, Pana JH (2018) Anatase and rutile in evonik aeroxide P25: Heterojunctioned or individual nanoparticles? Catal Today 300:12–17
61. Pohl S, Janka O, Füglein E, Kickelbick G (2021) Thermoplastic silsesquioxane hybrid polymers with a local ladder-type structure. Macromolecules 54:3873–3885